Coexistence of 5G With the Incumbents in the 28 and 70 GHz Bands

Seungmo Kim, Eugene Visotsky, *Member, IEEE*, Prakash Moorut, Kamil Bechta, Amitava Ghosh, *Fellow, IEEE*, and Carl Dietrich, *Senior Member, IEEE*

***Abstract*— A promising way of realizing the fifth generation (5G) wireless systems is to operate 5G deployments at higher frequency bands, specifically in the millimeter-wave (mmW) spectrum (30–300 GHz). Access to such spectrum bands will enable future 5G wireless systems to meet the 5G requirements of peak rate greater than 10 Gb/s, and cell edge rate of up to 1 Gb/s. However, the emerging 5G systems will need to coexist with a number of incumbent systems in these bands. This paper provides an extensive study of the co-channel coexistence of 5G in two critical mmW bands, 27.5–28.35 GHz (28 GHz) and 71–76 GHz (70 GHz) bands, where fixed satellite service (FSS) and fixed service (FS), such as wireless backhaul, are the predominant incumbent users. In the 28-GHz study, we show that interference from 5G into the FSS space stations can be kept below the FSS interference protection criterion. We also characterize the minimum separation distance between the FSS earth stations (ESs) and 5G in order to protect the 5G system from interference due to the ESs transmissions. In the 70-GHz study, we show that the 5G-to-FS interference could be a potential issue in certain scenarios, but we introduce techniques to significantly suppress this interference, while maintaining acceptable performance of the 5G systems. For each study, we suggest appropriate deployment strategies for a 5G system based on our results.**

***Index Terms*— 5G, coexistence, spectrum sharing, mmW, 28 GHz, 70 GHz, FSS, FS, wireless backhaul.**

I. Introduction

THE millimeter wave (mmW) bands previously have been best suited for satellite or fixed microwave applications. However, recent technological breakthroughs, such as the capability to integrate a very large numbers of antennas into future the 5th generation (5G) User Equipments (UEs) and Access Points (APs), have newly enabled advanced mobile services in these bands, notably including very high speed and low latency services [5]. Thus, disadvantages in propagation due to high frequency in mmW bands can be mitigated by using large antenna arrays at both transmitter and receiver ends of 5G wireless links, creating a massive Multiple Input-Multiple Output (MIMO) communication system. The ideas of deploying massive MIMO arrays in mmW bands have been well-covered in recent work such as [2] and [3].

There is high international interest (including USA, Japan and South Korea) in making the 27.5-28.35 GHz (28 gigahertz, GHz) band available for mobile use [5]. In addition, the 71-76 GHz (70 GHz) band was identified at the International Telecommunication Union (ITU)'s World Radiocommunication Conference (WRC) 2015 [6] as a possible band for future 5G wireless system deployments. In the 28 GHz band, Fixed Satellite Service (FSS) uplink–i.e., the communication links from Earth Stations (ESs) to Space Stations (SSs)–is in wide use, whereas in the 70 GHz band, the Fixed Service (FS) Wireless Backhaul (WB) for other cellular systems–e.g., the 4th generation (4G)–is the predominant incumbent.

There is related work that discusses various models of coexistence [7]–[14], and a body of prior work that discusses the techniques of interference reduction [15]–[19]. There is also recent work that has been performed in the area of spectrum sharing in mmW bands [20]–[26].

In this paper, we discuss coexistence between 5G and two incumbents at 28 GHz and 70 GHz, the FSS and FS systems, respectively. Showing that 5G can coexist with these incumbent systems is critical to the introduction of 5G in mmW bands. One relevant discussion of the coexistence of the 5G systems is provided in [21]. Our work is more extensive than [21] for the following three reasons. Firstly, we discuss both co-channel interference scenarios of 5G-to-FSS and FSS-to-5G at 28 GHz, whereas in [21] only FSS ES-to-5G interference is discussed. In fact, the authors identified analysis of the 5G-to-SS interference as their future work. Secondly, we additionally study coexistence of 5G with FS at 70 GHz. Thirdly, motivated by our results at 70 GHz, we propose several techniques that mitigate interference from 5G APs and UEs to the incumbent systems while interference mitigation at 70 GHz is another future work area that is identified in [21].

The proposed interference mitigation schemes in this work are novel for several reasons. Firstly, while the prior schemes [23]–[25], [25] focus on inter-cell interference in 5G systems, we address coexistence of 5G with incumbent systems. Secondly, our schemes are more efficient than those proposed in [15]–[18], since (i) they are standalone techniques in the sense that they do not require assistance from infrastructure, such as the Spectrum Access System (SAS) adopted as a solution for coexistence at 3.5 GHz [4], and (ii) they are straightforward to implement in realistic deployments, as the proposed schemes solely rely on the native beam management protocols defined

Manuscript received December 18, 2016; revised March 2, 2017; accepted March 02, 2017. Date of publication April 12, 2017; date of current version June 1, 2017. *(Corresponding author: Seungmo Kim.)*

S. Kim and C. Dietrich are with the Department of Electrical and Computer Engineering, Virginia Polytechnic Institute and State University, Blacksburg, VA 24061, USA (e-mail: seungmo@vt.edu).

E. Visotsky, P. Moorut, and A. Ghosh are with the Nokia Bell Labs, Arlington Heights, IL 60004, USA.

K. Bechta is with the Nokia Bell Labs, 53-661 Wrocław, Poland.

Color versions of one or more of the figures in this paper are available online at http://ieeexplore.ieee.org.

Digital Object Identifier 10.1109/JSAC.2017.2687238

as part of the 5G air interface. Thirdly, this paper discusses detailed methods of compensating the performance degradation of 5G systems incurred when mitigating 5G interference towards the incumbent systems. Finally, this paper assesses the UE-to-FS interference that is not discussed in [18] and [19], and proposes a novel method of mitigating it.

Specifically, the contributions of this paper are as follows:

- We provide detailed analysis and supporting simulation results of the co-channel coexistence between 5G and uplink FSS systems in the 28 GHz band. With respect to the 5G system modeling, we concentrate on APs, as interference generated and observed at the APs is much more significant than that at the UEs. Hence, we analyze the AP-to-SS and ES-to-AP interference. Based on our results, we conclude that (i) potentially on the order of hundreds to thousands of APs can simultaneously transmit in a given 5G service area without harming an SS receiver and (ii) a separation distance on the order of a few kilometers is required between an ES and the 5G system for acceptable operation of 5G.
  We also provide an initial set of results on the UE-to-SS interference assessment. In general, characterization of the UE-to-SS interference is heavily dependent on the deployment scenario and such system parameters as the percentage of UEs indoors or below clutter, as well as the particulars of the UE antenna array design. Hence, a detailed study of the UE-to-SS interference is outside the scope of this paper. Nevertheless, we provide a number of preliminary results on UE-to-SS interference, indicating that under reasonable UE deployment assumptions, the number of active UEs supported can far exceed the number of active APs in a 5G service area.
- We analyze the co-channel coexistence between 5G and FS at 70 GHz. We assume the FS system to be a point-to-point WB for another cellular system such as 4G. Unlike the coexistence at 28 GHz, all of the four directions of interference are possible in this band: AP to FS, FS to AP, UE to FS, and FS to UE. It is because: (i) both directions of an FS link operate at 70 GHz, and (ii) UE has higher probabilities of Line-of-Sight (LoS) in a 5G-FS coexistence topology since the beam of an FS's antenna is placed terrestrially and pointed closer toward the ground. We find that compared to the FS-to-5G interference, the one from 5G to FS (both AP to FS and UE to FS) is more significant since an interference is aggregated among multiple cells.
- Motivated from the finding, we propose techniques that mitigate AP-to-FS and UE-to-FS interference. The main idea for mitigation of the AP-to-FS interference is to establish exclusion zones at each region of AP, in order to ensure that the transmit beam gain toward the FS is attenuated sufficiently. Mitigation of the UE-to-FS interference is to force a UE to generate an uplink beam that is away enough from the direction toward FS. The proposed techniques can be applied to other coexistence situations, as long as the incumbent system operates terrestrially.

The coexistence models adopted in this paper rely on realistic channel and beamforming models that strive to truthfully capture the interaction between the multipath environment observed at the APs and UEs (according to the channel model of [35]) and the selection process of the AP and UE transmit and receive beamforming weights. Given the selected weights, the resulting distribution of the AP and UE transmit and receive beamforming gains is central for characterizing the interference scenarios considered in this paper. Unfortunately, the multipath fading model in [35] is stochastic in nature and is quite complex, which makes closed-form mathematical analysis of the interference distributions of interest intractable. Thus, in this work we resort to a semi-analytical approach, whereby the interference distributions of interest are evaluated via Monte-Carlo simulations.

This paper is organized as follows. In Section II, we discuss coexistence of 5G with FSS at 28 GHz. Section III studies coexistence of 5G with FS at 70 GHz. Section IV describes our proposed techniques that mitigate interference from 5G to the incumbent system, followed by evaluation results in Section V. Conclusions are drawn in Section VI.

II. Coexistence of 5G With Fixed Satellite Service at 28 GHz

At 28 GHz, the FSS operates in the uplink only (from ES to SS). Therefore, for coexistence with 5G, the possible scenarios of interference are 5G to SS and ES to 5G. Note that we consider the case of co-channel interference only.

In general, we expect APs to be the dominant source of interference from 5G. The reason is that in comparison to AP-to-SS interference, the UE-to-SS interference has much smaller impact since the Effective Isotropically Radiated Power (EIRP) of a UE is likely far lower than that of an AP. In addition, a UE is far more likely than an AP not to have a line-of-sight (LoS) propagation path toward an SS, which further reduces the potential for the UE-to-SS interference. These observations are confirmed by our results on the UE-to-SS interference, indicating that the number of active UEs permitted in a 5G service area far exceeds that of active APs.

For the FSS-into-5G direction, only ES-to-AP interference is considered as interference observed at the APs is expected to be the bottleneck for 5G system deployments. The UEs likely to have smaller antenna gains and experience much higher propagation losses from the ES transmitters than APs. Hence, the directions of interference that we consider in this study are AP-to-SS, UE-to-SS and ES-to-AP.

Finally, we note that the distribution of UEs in the system plays an important role in both directions of the interference. The reason is that the position of a UE determines the UE's and the serving AP's beamforming directions, which in turn affects both the AP-to-SS, UE-to-SS and ES-to-AP interference. As in Table I, the cell site of an AP is divided into three sectors, each of which spans 120 degrees (°). The distribution of UEs follows Poisson Point Process (PPP) [27] in a sector region.

TABLE I
PARAMETERS FOR 5G

Parameter	AP	UE
Carrier frequency	28 GHz	
System layout	UMi [35]	
Inter-site distance (ISD)	200 m	
Cell density	29 cells/km^2	
Cell sectorization	3 sectors/site	
Duplexing	Time-division duplexing (TDD)	
Transmission scheme	Singler-user (SU)-MIMO	
Bandwidth	850 MHz	
Temperature	290 K	
Max antenna gain	5 dBi per element	
Transmit power	21 dBm per element	14 dBm per element
Number of antennas ($\lambda/2$ array)	8×8 and 16×16	4×4
Noise figure	7 dB	9 dB
Antenna height	10 m	1.5 m

TABLE II
PARAMETERS FOR FSS SS

Parameter	Class 1	Class 2	Class 3
Elevation angle (degrees)	15-55	15-55	5-50
Orbit distance (km)	36,000	36,000	9,000
Max antenna gain (dBi)	58	58	27
Temperature (K)	1000	650	570
Thermal noise (dBm/Hz)	-168.6	-170.5	-171.0
Path loss models between 5G and FSS SS (dB)	LoS: FSPL + 4 NLoS: FSPL + 24		
Interference protection criterion (I/N, dB)	$TH_{fss} = \{-12.2, -6, 0\}$		

TABLE III
RESULTS OF 5G AP-TO-FSS SS INTERFERENCE

SS class, Los/NLoS mix		Result			
		Mean individual-sector interference (dBm/Hz)	Maximum number of simultaneously transmitting sectors		
			TH_{fss} = -12.2 dB	6 dB	0 dB
AP EIRP = 62 dBm/100 MHz (8 × 8 array)					
Class 1	50% LoS / 50% NLoS	-213	2,000	8,000	32,000
	25% LoS / 75% NLoS	-216	3,800	15,200	60,800
	10% LoS / 90% NLoS	-220	9,000	36,000	144,000
Class 2	50% LoS / 50% NLoS	-213	1,200	4,800	19,200
	25% LoS / 75% NLoS	-216	2,300	9,200	36,800
	10% LoS / 90% NLoS	-220	5,400	21,600	86,400
Class 3	50% LoS / 50% NLoS	-217	2,200	8,800	35,200
	25% LoS / 75% NLoS	-219	4,400	17,600	70,400
	10% LoS / 90% NLoS	-223	10,000	40,000	160,000
AP EIRP = 74 dBm/100 MHz (16 × 16 array)					
Class 1	50% LoS / 50% NLoS	-213	2,000	8,000	32,000
	25% LoS / 75% NLoS	-216	3,800	15,200	60,800
	10% LoS / 90% NLoS	-220	9,000	36,000	144,000
Class 2	50% LoS / 50% NLoS	-213	1,200	4,800	19,200
	25% LoS / 75% NLoS	-216	2,300	9,200	36,800
	10% LoS / 90% NLoS	-220	5,400	21,600	86,400
Class 3	50% LoS / 50% NLoS	-211	600	2,400	9,600
	25% LoS / 75% NLoS	-214	1,300	5,200	20,800
	10% LoS / 90% NLoS	-218	3,000	12,000	48,000

TABLE IV
RESULTS OF 5G UE-TO-FSS SS INTERFERENCE

SS class, Los/NLoS mix		Result			
		Mean individual-UE interference (dBm/Hz)	Maximum number of simultaneously transmitting UEs		
			TH_{fss} = -12.2 dB	6 dB	0 dB
Class 1	25% LoS / 75% NLoS	-225	283,000	1,132,000	4,528,000
	10% LoS / 90% NLoS	-228	566,000	2,264,000	9,056,000
	100% NLoS	-238	6,226,000	24,904,000	99,616,000
Class 2	25% LoS / 75% NLoS	-217	28,000	112,000	448,000
	10% LoS / 90% NLoS	-220	57,000	228,000	912,000
	100% NLoS	-230	627,000	2,508,000	10,032,000
Class 3	25% LoS / 75% NLoS	-223	64,400	257,800	1,031,200
	10% LoS / 90% NLoS	-227	162,000	648,000	2,591,800
	100% NLoS	-237	1,781,900	7,127,500	28,510,100

A. Interference From 5G AP and UE to FSS SS

1) System Model: Tables I and II provide parameters for the 5G AP/UE and FSS SS, respectively. For the SS, the interference protection criterion is defined as the threshold of interference-to-noise ratio (I/N), which is denoted by TH_{fss}. Regarding the path loss between an AP/UE and an SS, various combinations of LoS and Non-Line-of-Sight (NLoS) channel conditions are considered. Note that a large percentage of LoS sites appears to be unrealistic given real-world vegetation/foliage losses and practical deployment cases of 5G. Moreover, we note that LoS channel conditions will occur with very low probabilities at 28 GHz, where propagation of a microwave signal is adversely affected not only by blockage due to buildings and other structures but also by vegetation. Therefore, only realistic subsets of LoS/NLoS combinations are reported in our final results given in Tables III and IV.

The path loss models are elaborated as follows. In LoS conditions, we assume a free space path loss (FSPL) model [28] plus additional atmospheric and polarization losses of 4 dB In the NLoS channel conditions, an FSPL model is again used, with additional 20 dB of clutter loss in addition to the 4 dB of atmospheric and polarization losses [29]. Thus, the total additional loss assumed in the NLoS model is 24 dB. Recall that *clutter loss* is the loss due to various conditions on the terrain (such as buildings) over a wide area, and hence it also accounts for the *diffraction loss* [30], which is the loss due to propagation bending around an object such as a building or a wall. Note that our assumption of a 20 dB of clutter loss is worst case with respect to interference modeling, as diffraction losses can be significantly higher depending on the ray angles of incidence and departure toward the satellite. This potentially higher clutter loss may result in an even lower AP/UE-to-SS interference in practice.

The threshold TH_{fss} of -12.2 dB in Tables III and IV is derived from [31]. There is, however, general recognition in the satellite community that this interference level was developed when satellite networks were considered to be power limited, whereas today satellite networks tend to be interference limited and, as such, this protection level is very conservative [6]. Therefore more realistic and less stringent protection criteria of TH_{fss} of -6 dB and 0 dB are used in this paper. It is to be noted that TH_{fss} of -6 dB and 0 dB corresponding to 1dB and 3 dB desensitization (desense) interference thresholds, which represent the increase in the noise floor of the system due to interference, are also typically used for mobile terrestrial systems [32], [33]. We use the same -6 dB and 0 dB I/N as the protection criteria for satellite systems in addition to -12.2 dB, since without the knowledge of the receiver characteristics of the satellite systems, it is difficult to derive a more precise value of the I/N protection criteria for the FSS SS and ES receivers. For 5G, TH_{5g} of -12.2 dB was also used in addition to -6 dB and 0 dB to be consistent with the FSS interference results.

2) Analysis of Interference: As a metric that measures AP/UE-to-SS interference, we calculate the number of simultaneously transmitting APs/UEs such that TH_{fss} at the FSS SS is not violated.

Here we provide an analysis framework for the AP-to-SS interference. With straightforward modifications, this framework can be also applied to the UE-to-SS interference. To compute such an aggregate interference, an interference from the downlink transmission of a single sector is computed by averaging over all possible downlink directions according

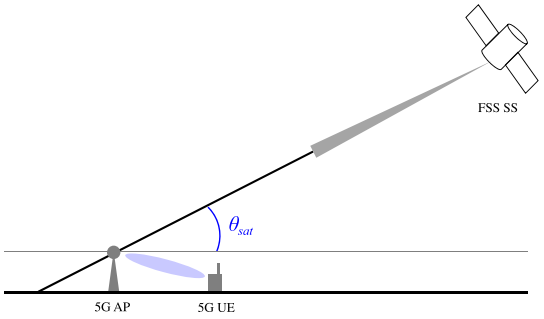

Fig. 1. Topology of coexistence between a 5G system and an FSS SS on elevation plane.

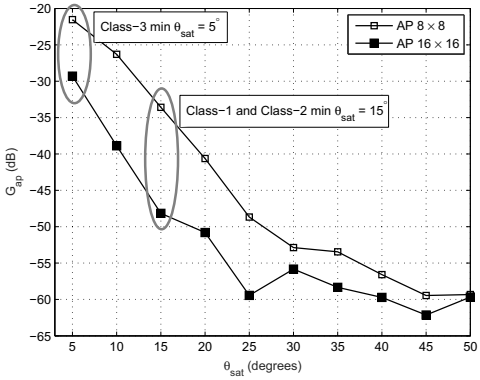

Fig. 2. Normalized mean AP antenna gain into FSS SS vs. the elevation angle θ_{sat}.

to position of the UE, which is given by

$$I_{5g} = \frac{1}{\left|\mathcal{R}_k^2\right|} \int_{\mathbb{x}_{ue}^{(k)} \in \mathcal{R}_k^2} \frac{P_{T,ap} G_{ap,a}(\mathbb{x}_{ue}) G_{ap,e}(\mathbb{x}_{ue}) G_{ss,3db}}{PL_{ap \to ss}} d\mathbb{x}_{ue} \tag{1}$$

where $\mathcal{R}_k^2$ is region of a sector and thus $\left|\mathcal{R}_k^2\right|$ is the area of a sector; $\mathbb{x}_{ue}$ is position of a UE in an $\mathcal{R}_k^2$; $P_{T,ap}$ is transmit power of an AP; $G_{ap,a}$ and $G_{ap,e}$ are the azimuth and elevation beamforming gains of a downlink transmission to a UE in the direction toward the SS; $G_{ss,3db}$ is the beamforming gain of the SS receiver antenna within its 3dB-contour; $PL_{ap \to ss}$ is the path loss between the AP and the SS.

For a 5G AP, the attenuation patterns of an antenna element on the elevation and azimuth plane are given by [35]

$$\begin{aligned} A_a(\phi) &= \min\left\{12\left(\frac{\phi}{\phi_{3db}}\right)^2, A_m\right\}, \\ A_e(\theta) &= \min\left\{12\left(\frac{\theta - 90^\circ}{\theta_{3db}}\right)^2, A_m\right\} \ \text{[dB]} \end{aligned} \tag{2}$$

where ϕ and θ are angles of a beam on the azimuth and elevation plane, respectively; $(\cdot)_{3db}$ denotes an angle at which a 3-dB loss occurs. Then the antenna element pattern that is combined in the two planes is given by

$$A(\theta, \phi) = \min\left(A_a(\phi) + A_e(\theta), A_m\right) \ \text{[dB]} \tag{3}$$

where A_m is a maximum attenuation (front-to-back ratio). It is defined $A_m = 30$ dB in [35], but it can be higher in practice. Finally, an antenna gain that is formulated as

$$G(\phi, \theta) = G_{max} - A(\phi, \theta) \ \text{[dB]} \tag{4}$$

where G_{max} is a maximum antenna gain.

Note that $G_{ap,a}$ and $G_{ap,e}$ are lower than the maximum azimuth and elevation beamforming gains. The reason is depicted in Fig. 1. Generally, a beam of an AP is pointed away from an SS since transmitting to a UE that is placed at a lower elevation than the AP. The elevation angles that are shown in Table II for each class of SS [29] are obtained in this manner.

Based on (1), we calculate an *aggregate* interference, which is given by

$$I_{aggr}\left(\mathbb{N}[\mathcal{S}_{5s}]\right) = I_{5g} \times \mathbb{N}[\mathcal{S}_{5s}] \tag{5}$$

where $\mathcal{S}_{5s}$ is a set of 5G sectors; $\mathbb{N}[\cdot]$ is the number of elements in a set. Now, we can obtain the number of simultaneously transmitting APs, $\mathbb{N}[\mathcal{S}_{5s}]$, such that I_{aggr} does not exceed TH_{fss}, which is given by

$$\arg\max_{\mathbb{N}[\mathcal{S}_{5s}]} I_{aggr}\left(\mathbb{N}[\mathcal{S}_{5s}]\right) < 10^{0.1 TH_{fss}} \tag{6}$$

within an area that a satellite beam forms on the Earth surface. The receive antenna on board an SS forms a spot where a solid angle formed by the receive beam subtends the surface of the Earth; and this is typically known as a *spot beam*. It is assumed that the entire 5G system deployment falls within the 3dB-contour of an SS receiver spot beam.

3) Evaluation of Interference: Tables III and IV record our final results of (i) a mean individual-sector/UE interference power received at an SS receiver, I_{5g}/W from (1) where W is bandwidth of 5G, and (ii) the maximum number of simultaneous 5G sectors/UEs that can transmit under a TH_{fss}, $\arg\max_{\mathbb{N}[\mathcal{S}_{5s}]} I_{aggr}\left(\mathbb{N}[\mathcal{S}_{5s}]\right)$ from (6). No specific interference control techniques were assumed at the UEs.

AP-to-SS Interference: Table III shows that potentially very large numbers of simultaneously transmitting sectors can be supported. For example, even using a very conservative -12.2 dB of TH_{fss}, Table III shows that with increased EIRP of an AP from 62 to 74 dBm/100 MHz, the number of active AP sectors that can simultaneously transmit is kept the same for both Class 1 and Class 2 FSS systems, although the number drops for Class 3 FSS systems. This result has certain implications on the deployment of 5G systems. Specifically, an environment with higher NLoS yields lower interference into an SS receiver, due to higher attenuation of the interfering signal power. In other words, a higher density of 5G sectors can be deployed in urban areas than in suburban areas.

Fig. 2 provides a justification for this drop. It depicts the *normalized* (assuming maximum antenna gain is normalized to 0 dBi) transmit antenna gain of a sector toward an SS, which is given by $G_{ap} = -A(\phi, \theta)$ from (4) with $G_{max} = 0$. In general, an AP has a lower antenna gain toward an SS with a larger antenna array, since the beamwidth is reduced with increasing number of transmit antennas. Conversely, the antenna gain toward an SS is increased with higher number of transmit antennas if an SS falls within the main beam of an AP. The main difference between Class 3 and the other two classes is the elevation angle θ_{sat}, as depicted in Fig. 1.

According to Table II, Class 3 SSs operate at a lower elevation angle than the other two classes, thus they experience higher interference due to increased transmit antenna count at the APs.

Due to several reasons, the numbers given in Table III likely underestimate the actual number of APs that could be deployed without violating TH_{fss}. Firstly, in real-world networks, it is unlikely that all 5G sectors simultaneously transmit. In fact, in current deployments, network loading rarely exceeds 30% [29], thus allowing a roughly three-fold increase in the number of sectors given in Table III without adversely impacting FSS links. Secondly, the results only consider *outdoor* deployments. Indoor APs will not contribute to aggregate interference levels observed at the SS receivers due to very high penetration losses that occur in mmW bands. Finally, this study assumes that all APs are synchronized and analyzes interference during a downlink period when all APs are in transmit mode. If geographically-adjacent network deployments of several operators are not synchronized, then their respective downlink periods will not occur simultaneously. Thus, even a smaller percentage of APs will be in transmit mode simultaneously, whereas the remainder of active APs will be receiving uplink transmissions from UEs. As transmission of a UE is expected to have much smaller impact on an SS, the overall interference from a 5G deployment area will be further reduced. In summary, fractional network loading, indoor deployments, and unsynchronized network deployments result in a more favorable scenario than what was modeled to obtain the results in Table III.

UE-to-SS Interference: Here we provide an initial set of results on the UE-to-SS interference. The interference calculation steps mirror those for the AP-to-SS interference given in (1)-(6), but with the UE parameters given in Table I. Namely, based on the statistics of the UE antenna array gains into an SS receiver, a per-UE average interference value is computed in Table IV. From that, the number of *simultaneously transmitting* UEs is derived, given a certain interference threshold at the SS. Note that unlike on the downlink where under heavily loaded APs continuously transmit, UE transmissions on the uplink are scheduled periodically, as all available uplink slots are shared between the active UEs in a 5G cell. Assuming a typical *heavy-load* approximation of 10 active UEs per sector, the number of *active* UEs per sector becomes roughly 10 times that of the simultaneously transmitting UEs. The final numbers of supported active UEs in a 5G deployment area under various LoS/NLoS channel conditions are given in Table IV. Note that the highest probability of LoS for the UE-to-SS links was assumed to be 25%.

We make two key observations on the UE-to-SS results: i) the number of active UEs supportable in a 5G system far exceeds the number of simultaneously transmitting APs given in Table III. This is mainly due to the increased probability of NLoS for the UEs and the intermittent nature of the UE uplink transmissions, where we have assumed a per UE transmission duty cycle of 10% to convert the number of simultaneously transmitting UEs into the number active UEs.; (ii) these results may still significantly underestimate the total number of active 5G UEs that can be supported in a 5G system, as a significant fraction the UEs may be situated indoors or inside vehicles and have very high path loss towards the SS receivers.

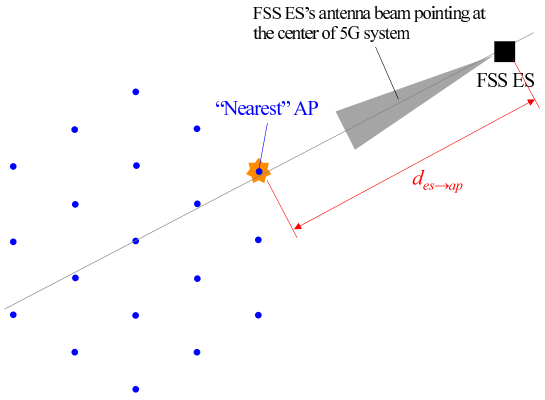

Fig. 3. Azimuth plane of a 5G-FSS ES coexistence topology.

B. Interference From FSS ES to 5G AP

1) System Model: The analysis is based on a link-level protection criterion that is defined as an I/N observed at a 5G AP receiver. Specifically for our results, the link-level protection thresholds, denoted by TH_{5g}, are set to -12.2, -6, and 0 dB of I/N. Based on the link-level protection criterion, we define a system-level interference protection criterion as the minimum distance between an FSS ES and the *edge* of the 5G system deployment, such that 95% of the 5G uplink connections in the cell nearest to the ES transmitter are protected under TH_{5g}. The distance to the edge of the system deployment is defined as the minimum distance between the ES and the 5G AP that is nearest to it. Fig. 3 illustrates an example of the 5G system layout and the definition of the minimum protection distance. The parameters used for this study refer to Table I. For the terrestrial propagation between an ES transmitter and APs, the following three models are assumed: FSPL [28], Urban Macro (UMa), and Rural Macro (RMa) [35].

Each AP activates an elevation and azimuth beam to receive the intended uplink transmission based on the preferred azimuth and elevation beam index feedback from the UE. Each UE selects its preferred elevation and azimuth beam from the elevation and azimuth codebook based on the long-term received power measurements obtained for all beams in the codebooks. For the results reported here, a codebook with 16 entries was used for beam selection in the azimuth and elevation dimensions. The beam patterns are symmetric in elevation and azimuth planes.

2) Analysis of Interference: Given the preferred azimuth and elevation beam, an interference received from an ES at a 5G AP is computed as

$$I_{es} = \frac{P_{T,es} G_{es,a} G_{ap,a}\left(\mathrm{x}_{ue}\right) G_{ap,e}\left(\mathrm{x}_{ue}\right)}{PL_{es\rightarrow ap}\left(d_{es\rightarrow ap}\right)} \tag{7}$$

where the parameters are defined in the same manner as in (1). The transmit power of the ES node is denoted by $P_{T,es}$. The azimuth pattern of an ES, $G_{es,a}$, is defined in [34]. For the interference analysis, the value of $EIRP_{es} = P_{T,es} + G_{max,es}$

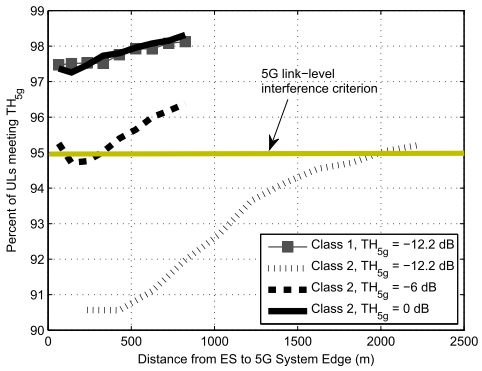

Fig. 4. 5G uplinks with Classes 1 and 2 ES under FSPL.

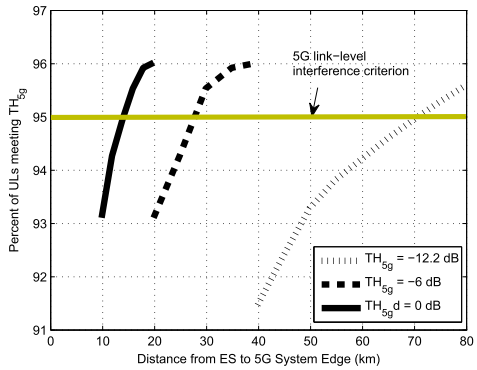

Fig. 5. 5G uplinks with Class 3 ES under FSPL.

(where $G_{max,es}$ is the maximum transmit antenna gain for the ES node) is specified according to the three classes of ES transmitters [29] given by: 12.2, 24.1, and 48 dBm/MHz for Class 1, 2, and 3, respectively.

Given a certain level of $EIRP_{es}$ and position of the ES relative to the 5G system layout, an ES-to-5G interference is calculated for every UE attached to the *nearest* AP. Each calculation is performed with randomized positions of the UEs in the system and randomized positions of the ES around the 5G system layout, with variation of $d_{es\rightarrow ap}$. It is assumed that the ES antenna azimuth is always directed toward the center of the 5G system layout.

3) Evaluation of Interference: Figs. 4 and 5 demonstrate cumulative distribution functions (CDFs) of the uplink connections computed over all UE positions in the nearest cell as a function of $d_{es\rightarrow ap}$ for Classes 1 and 2, and for Class 3, respectively. Given the 95% protection target, the minimum $d_{es\rightarrow ap}$ can be determined from Figs. 4 and 5. As evident in the figures, the required $d_{es\rightarrow ap}$ is highly dependent on TH_{5g} as well as $EIRP_{es}$ toward the 5G system.

Based on the above results, we observe that the required values of $d_{es\rightarrow ap}$ are reasonable in most cases of interest and will not place an overly restrictive set of constraints on future 5G system deployments. With a protection margin of -6 dB I/N, the distance where less than 5% of links fall below the protection threshold TH_{5g} is less than 400 m for Class 2 ESs and less than 50 m for Class 1 ESs. While our calculations show that Class 3 ESs nominally could interfere with 5G systems at a distance of 28 km with a -6 dB of I/N threshold, we believe that this distance could be significantly smaller in practice due to additional clutter loss between 5G APs and ES transmitters not accounted in the FSPL model.

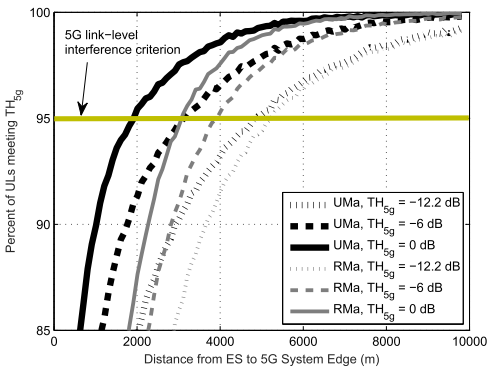

Fig. 6. 5G uplinks with Class 3 ES under UMa and RMa.

TABLE V
REQUIRED SEPARATION DISTANCE UNDER UMa AND RMa

	UMa			RMa		
TH_{5g} (dB)	-12.2	-6	0	-12.2	-6	0
Required $d_{es\rightarrow ap}$ (m)	4,900	3,000	2,000	5,100	4,000	3,000

To more accurately model the terrestrial propagation effect, such as the clutter loss, we also generated results using the 3GPP UMa and RMa models [35] for Class 3 ES transmitters. The 3GPP UMa and RMa path loss models exhibit much higher path loss exponents than the FSPL and are more appropriate for terrestrial propagation modeling. Fig. 6 exhibits the percent of 5G uplinks below TH_{5g} in presence of interference from an FSS ES based on Class 3. Compared to Fig. 5, $d_{es\rightarrow ap}$ is dramatically reduced. This implies that a 5G system experiences lower interference from an ES when deployed in an environment with higher attenuation–mainly due to higher probability of NLoS propagation conditions.

Table V shows the results with both 3GPP path loss models for Class 3 ES transmitters for various I/N thresholds. As expected, the RMa model requires a larger distance for interference protection, since in general it predicts higher LoS probability as a function of distance and has a lower path loss exponent than UMa. Specifically, the table indicates that the worst case of protection distance of 5,100 m occurs with RMa and the most restrictive threshold of TH_{5g} (-12.2 dB).

III. COEXISTENCE OF 5G WITH FIXED SERVICE AT 70 GHz

In this section, we discuss co-channel coexistence of 5G at 70 GHz where the Fixed Service (FS) is the incumbent system. We consider a point-to-point Wireless Backhaul (WB) system that adopts highly directional antennas to connect distant radio towers. Note that the FS system provides backhaul for another cellular system, thus it is uncoordinated with the 5G.

Unlike the 28-GHz coexistence problem, there are four possible interference scenarios: FS to AP, AP to FS, FS to UE, and UE to FS. The reasons are as follows: (i) both directions of an FS system's wireless link transmit in the 70 GHz band; (ii) a UE has higher probability of LoS than in the coexistence

TABLE VI
PARAMETERS FOR 70-GHz COEXISTENCE

Parameter	5G		FS
Carrier frequency	73.5 GHz		
Path loss model [35]	UMa and UMi		
Bandwidth	1 GHz		
System	AP	UE	WB
Transmit power	15 dBm per element	14 dBm per element	19 dBm
Max antenna gain	8 dBi per element	5 dBi per element	50 dBi
Temperature	290 K	290 K	290 K
Noise figure	7 dB	9 dB	5 dB
Antenna height	10 m	1.5 m	25 m
Number of antennas	8×8 and 16×16 ($\lambda/2$ array)	Omni and 4×4 ($\lambda/2$ array)	

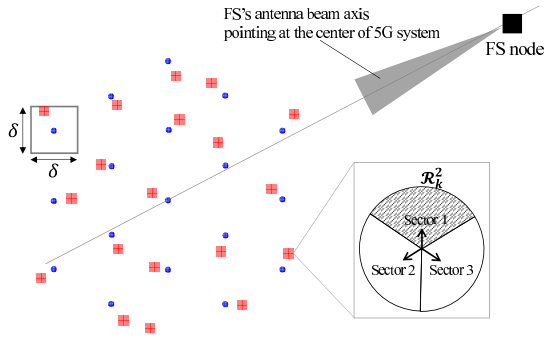

Fig. 7. Topology of a 5G-FS coexistence.

at 28 GHz since the beam of an FS's antenna is placed terrestrially and pointed closer toward the ground.

Note that this analysis framework is sufficiently general in that it can be readily applied to coexistence scenarios between 5G and other terrestrial incumbent system.

A. System Model

The parameters for 5G and FS are summarized in Table VI. Note that the parameters of 5G are different from the ones used in the 28 GHz coexistence of Section II. Since the rules are still under discussion by the FCC for the 70 GHz band, the parameters are obtained from a standard 3GPP evaluation model [37]. We assume 19 cell sites–equivalently 19 APs–where in total $\mathbb{N}[\mathcal{S}_{5s}] = 57$ sectors exist.

Fig. 7 describes a *drop*–or an instance–of topology for coexistence. There are two important assumptions: (i) the FS node is regarded as a transmitter in an FS-to-5G interference scenario while it is a receiver in a 5G-to-FS interference situation; (ii) the FS node points its beam at the center of the 5G system. The interference between the 5G and the FS nodes is a function of at least four variables corresponding to the positions of transmitters and receivers in the interferer and victim systems. Since the FS node is always assumed to point its beam at the center of the 5G system, position of the FS receiver in the FS-to-5G scenario and position of FS transmitter in the 5G-to-FS scenario can be excluded from consideration. In Fig. 7, the FS node is placed outside of the 5G system, at 176 different positions on an r-θ coordinate: $r = [0 : 500 : 10, 500]$ and $\theta = [0 : \frac{\pi}{4} : \frac{7\pi}{4}]$ in reference to the center of the 5G system.

The blue circles in Fig. 7 correspond to positions of the APs in a classical hexagonal cell layout with Inter-Site Distance (ISD) of 200 m. The actual positions of APs (red squares) are *dithered* within δ m relative to the locations of the hexagonal cells, to achieve a more realistic system layout. Furthermore, we uniformly and randomly distribute 10 UEs in the kth sector region, denoted by $\mathcal{R}_k^2$. The distribution of UEs can be modeled as a homogeneous PPP [27] whose density is kept constant to be $\lambda_{ue} = 10$ over $\mathcal{R}_k^2, k = 1, 2, \cdots, \mathbb{N}[\mathcal{S}_{5s}] = 57$.

For the path loss model, we use the 3GPP UMa and UMi [35]. The models are used both for the 5G-FS and AP-UE links. Again, although 3GPP defines path loss models for outdoor and indoor scenarios, this paper discusses the 5G placed outdoor only since the FS devices are likely placed outdoors and penetration losses at 70 GHz are very high.

The antenna element pattern for the 5G system refers to (2) through (4) in Section II-A. The antenna beam pattern for an FS device is provided in [36] as

$$G_{fs}(\theta) = \begin{cases} G_{max} - 2.5\times10^{-3}\left(\frac{D}{\lambda}\theta\right)^2, & 0^\circ < \theta < \theta_m \\ G_1, & \theta_m \le \theta < \theta_r \\ 32 - 25\log\theta, & \theta_r \le \theta < 48^\circ \\ -10, \ [\text{dB}] & 48^\circ \le \theta \le 180^\circ \end{cases} \tag{8}$$

where G_{max} is a maximum gain; D is antenna diameter; λ is a wavelength; $G_1 = 2 + 15\log\frac{D}{\lambda}$: gain of the first sidelobe; $\theta_m = \frac{20\lambda}{D}\sqrt{G_{max} - G_1}$ in degrees; $\theta_r = 15.85\left(\frac{D}{\lambda}\right)^{-0.6}$ in degrees.

B. Analysis of Interference

1) Coexistence Topology: We now discuss a general framework for interference analysis that is applicable to all the four scenarios of interference, where the key is to analyze how antenna gains are determined for: (i) the interferer system's transmitters and (ii) the victim system's receivers. Let $\mathrm{x} = (x, y)$ denote position of a node on a two-dimensional Cartesian coordinate plane. Subscripts "i" and "v" indicate the "interferer" and "victim", respectively, and "t" and "r" denote "transmitter" and "receiver", respectively. Without loss of generality, we consider the AP-to-FS interference where $\mathrm{x}_{i,t}$, $\mathrm{x}_{i,r}$, and $\mathrm{x}_{v,r}$ denote the positions of an AP, a UE, and the FS receiver respectively. The method can be extended to the other scenarios (i.e., FS to AP, UE to FS, and FS to UE).

Fig. 8 illustrates the azimuth plane of an AP-to-FS interference scenario. There are two angles that determine the interference level between a 5G AP and the FS node: the off-axis angle, ϕ_{off}, and the steering angle, ϕ_{str}. A ϕ_{str} is an angle between the direction of a beamforming and the antenna's physical orientation. Such an electrical steering is only assumed for the 5G (i.e., APs and UEs), whereas the FS assumed to be equipped with fixed beam antennas. Also, we define an *interference axis* to be a line connecting the interfering transmitter (the AP) and the victim receiver (the FS receiver). A ϕ_{off} is an angle between the direction of a beamforming and the interference axis. These angles will be used in the analysis to represent discrimination of antenna gain from: (i) electrical steering and (ii) pointing away from the FS receiver, respectively.

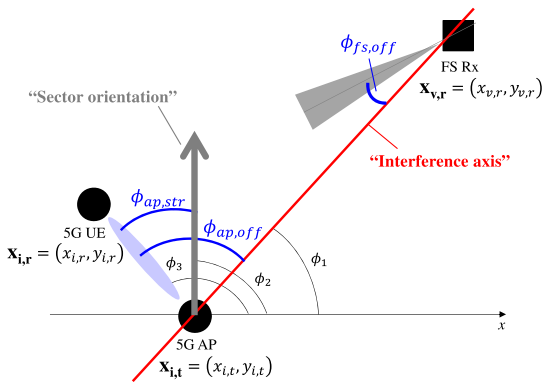

Fig. 8. 5G AP as interferer on the azimuth plane (Cell orientation of 90°).

For defining the angles, we put an azimuth-plane geometry on a quadrant and set $\mathrm{x}_{i,t}$ at the origin of the quadrant. The angle formed by the interference axis with respect to the X-axis is denoted by ϕ_1. The angle of a sector's physical orientation is denoted by and set as $\phi_2 = 90°$. The beamforming angle with respect to the X-axis of the quadrant is denoted as ϕ_3. Now we can define ϕ_{off} and ϕ_{str} for the 5G AP and FS receiver as

$$\phi_{ap,off}\left(\mathrm{x}_{i,t}, \mathrm{x}_{i,r}, \mathrm{x}_{v,r}\right) = \phi_3 - \phi_1 \tag{9}$$

$$\phi_{ap,str}\left(\mathrm{x}_{i,t}, \mathrm{x}_{i,r}\right) = \phi_3 - \phi_2 \tag{10}$$

$$\phi_{fs,off}\left(\mathrm{x}_{i,t}, \mathrm{x}_{v,t}, \mathrm{x}_{v,r}\right) = \arccos\left(\frac{\left(\mathrm{x}_{v,t} - \mathrm{x}_{v,r}\right) \cdot \left(\mathrm{x}_{i,t} - \mathrm{x}_{v,r}\right)}{\|\mathrm{x}_{v,t} - \mathrm{x}_{v,r}\| \|\mathrm{x}_{i,t} - \mathrm{x}_{v,r}\|}\right) \tag{11}$$

where $(\cdot)$ in (11) indicates a dot product between two vectors, and

$$\phi_1 = \arctan\left(\mathrm{x}_{v,r}, \mathrm{x}_{i,t}\right) = \arctan\left(\frac{y_{v,r} - y_{i,t}}{x_{v,r} - x_{i,t}}\right) \tag{12}$$

$$\phi_3 = \arctan\left(\mathrm{x}_{i,r}, \mathrm{x}_{i,t}\right) = \arctan\left(\frac{y_{i,r} - y_{i,t}}{x_{i,r} - x_{i,t}}\right). \tag{13}$$

Now, denote azimuth and elevation planes by subscripts "a" and "e," respectively. Then two types of attenuation, $A_{ap,a,off}\left(\phi_{ap,off}\right)$ and $A_{ap,a,str}\left(\phi_{ap,str}\right)$, can be obtained by substituting $\phi_{ap,off}$ and $\phi_{ap,str}$ into $A_a(\phi)$ in (2), where $\phi_{ap,off,3db} = 6°$ and $\phi_{ap,str,3db} = 65°$ [35].

Fig. 9 describes an elevation plane of the interference scenario of interest. Similarly to the azimuth-plane analysis, the off-axis angles of the interfering transmitter and the victim receiver, $\theta_{ap,off}$ and $\theta_{fs,off}$, are defined with respect to the interference axis. The angles can be calculated based on locations and heights, which are given by

$$\theta_{ap,off} = \arctan\left(\frac{h_{v,r} - h_{i,t}}{\|\mathrm{x}_{v,r} - \mathrm{x}_{i,t}\|}\right) + \theta_{ap,str} \tag{14}$$

$$\theta_{fs,off} = \arctan\left(\frac{h_{v,r} - h_{v,t}}{\|\mathrm{x}_{v,r} - \mathrm{x}_{v,t}\|}\right). \tag{15}$$

Note that although it is set $h_{v,t} = h_{v,r}$ in Fig. 9, it can be generalized as in (15). Again, by substituting $\theta_{ap,off}$ into $A_e(\theta)$ in (2), we can obtain $A_{ap,e,off}\left(\theta_{ap,off}\right)$ with $\theta_{ap,off,3db} = 6°$ and $\theta_{ap,str,3db} = 65°$ [35].

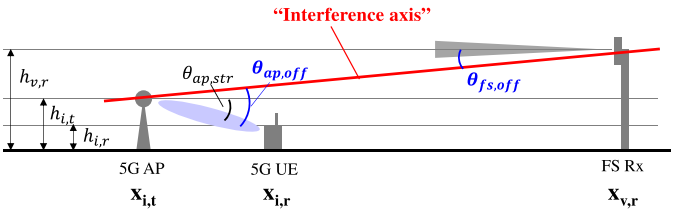

Fig. 9. 5G AP as interferer on the elevation plane.

Also, for the FS receiver, the azimuth and elevation off-axis angles, $\phi_{fs,off}$ and $\theta_{fs,off}$, are substituted into (8) to obtain the $G_{fs}\left(\phi_{fs,off}\right)$ and $G_{fs}\left(\theta_{fs,off}\right)$.

2) Analysis Framework: An interference power received at a victim receiver is computed as

$$I = \frac{P_T G_i\left(\phi_i, \theta_i\right) G_v\left(\phi_v, \theta_v\right)}{PL\left(\mathrm{x}_{i,t}, \mathrm{x}_{v,r}\right)} \tag{16}$$

where P_T denotes a transmit power of the interferer system's transmitter; $G(\cdot)$ denotes an antenna gain that is given in (4). Again, for a 5G device (either AP or UE), the angles $\phi_{i \text{ or } v}$ and $\theta_{i \text{ or } v}$ include ϕ_{off} and ϕ_{str}, and θ_{off} and θ_{str}. It is important to note that although not explicitly expressed, an I is a function of $\left(\mathrm{x}_{i,t}, \mathrm{x}_{v,t}, \mathrm{x}_{v,r}\right)$ in an FS-to-5G interference and $\left(\mathrm{x}_{i,t}, \mathrm{x}_{i,r}, \mathrm{x}_{v,r}\right)$ in a 5G-to-FS interference, which can be expressed through (9) and (11) and written as

$$I = \begin{cases} I_{fs\to ap}\left(\mathrm{x}_{i,t}, \mathrm{x}_{v,t}, \mathrm{x}_{v,r}\right) \\ I_{ap\to fs}\left(\mathrm{x}_{i,t}, \mathrm{x}_{i,r}, \mathrm{x}_{v,r}\right). \end{cases} \tag{17}$$

Also, $PL(\cdot)$ is a path loss that is a function of $\mathrm{x}_{i,t}$ and $\mathrm{x}_{v,r}$. By generalizing an expression for path loss given in [35] as $PL = \xi d^{\alpha}$ where d is a distance, one can rewrite (16) as

$$I = P_T G_i\left(\phi_i, \theta_i\right) G_v\left(\phi_v, \theta_v\right) \xi^{-1} \|\mathrm{x}_{i,t} - \mathrm{x}_{v,r}\|^{-\alpha}. \tag{18}$$

3) 5G as Interferer: Based on (18), we can calculate 5G-to-FS interference. The analysis focuses on the AP-to-FS interference only but can readily be extended to the UE-to-FS scenario. We consider an aggregate AP-to-FS interference with the 5G system that is fully loaded in both downlink and uplink. An aggregate interference is defined as an interference that is received at a *victim* FS receiver at $\mathrm{x}_{v,r}$ from all the 5G sectors, which can be formulated as

$$\begin{aligned} I_{aggr} &= \sum_{k=1}^{\mathbb{N}[\mathcal{S}_{5s}]} I_{ap\to fs}^{(k)}\left(\mathrm{x}_{i,t}^{(k)}, \mathrm{x}_{i,r}^{(k)}, \mathrm{x}_{v,r}\right) \\ &= P_T \xi^{-1} \sum_{k=1}^{\mathbb{N}[\mathcal{S}_{5s}]} G_i^{(k)}\left(\phi_i, \theta_i\right) G_v^{(k)}\left(\phi_v, \theta_v\right) \|\mathrm{x}_{i,t}^{(k)} - \mathrm{x}_{v,r}\|^{-\alpha} \end{aligned} \tag{19}$$

where a superscript (k) indicates that the quantity is defined for a sector region, $\mathcal{R}_k^2$; a set of AP sectors is denoted by $\mathcal{S}_{5s}$.

Now we need to compute the mean of aggregate interference over all the possible positions of $\mathrm{x}_{i,t}^{(k)}$, $\mathrm{x}_{i,r}^{(k)}$ and $\mathrm{x}_{v,r}$, which is

given by

$$\begin{aligned}
&\bar{I}_{aggr} \\
&= \mathbb{E}\left[I_{aggr}\right] \\
&= \underbrace{\frac{1}{\mathbb{N}\left[\mathcal{S}_{fs}\right]} \sum_{\mathcal{S}_{fs}}}_{\text{average of } \mathrm{x}_{v,r}} \sum_{k=1}^{\mathbb{N}[\mathcal{S}_{5s}]} \underbrace{\frac{1}{\delta^2} \int_{\mathrm{x}_{i,t}^{(k)}}}_{\text{average of } \mathrm{x}_{i,t}^{(k)}} \underbrace{\frac{1}{\left|\mathcal{R}_k^2\right|} \int_{\mathrm{x}_{i,r}^{(k)} \in \mathcal{R}_k^2}}_{\text{average of } \mathrm{x}_{i,r}^{(k)}} \\
&\qquad \left(I_{ap \to fs}^{(k)}\right) d\mathrm{x}_{i,r}^{(k)} d\mathrm{x}_{i,t}^{(k)} \\
&= \frac{P_T \xi^{-1}}{\delta^2 \left|\mathcal{R}_k^2\right| \mathbb{N}\left[\mathcal{S}_{fs}\right]} \sum_{\mathcal{S}_{fs}} \sum_{k=1}^{\mathbb{N}[\mathcal{S}_{5s}]} \int_{\mathrm{x}_{i,t}^{(k)}} \int_{\mathrm{x}_{i,r}^{(k)} \in \mathcal{R}_k^2} \\
&\qquad \left(G_i^{(k)}\left(\phi_i, \theta_i\right) G_v^{(k)}\left(\phi_v, \theta_v\right) \left\|\mathrm{x}_{i,t}^{(k)} - \mathrm{x}_{v,r}\right\|^{-\alpha}\right) d\mathrm{x}_{i,r}^{(k)} d\mathrm{x}_{i,t}^{(k)}
\end{aligned} \tag{20}$$

where $\mathcal{S}_{fs}$ denotes a set of positions of the FS node. The integral expression in (20) is not amenable to analytic evaluation due to high complexity in calculation. Therefore, in the rest of the paper we evaluate (20) via Monte-Carlo simulations.

4) 5G as Victim: The FS-to-5G interference is a *per-sector* interference power averaged over the $\mathbb{N}[\mathcal{S}_{5s}] = 57$ sectors. As above and without loss of generality, we analyze the FS-to-AP interference scenario in detail, and this analysis is applicable to the FS-to-UE interference scenario by replacing parameters for the AP with those for the UE. From (19), the average interference that is received at an AP located at $\mathrm{x}_{v,r}^{(k)}$ and pointing its receive beam at a UE located at $\mathrm{x}_{v,t}^{(k)}$ in $\mathcal{R}_k^2$ can be formulated as

$$I_{avg} = \frac{1}{\mathbb{N}\left[\mathcal{S}_{5s}\right]} \sum_{k=1}^{\mathbb{N}[\mathcal{S}_{5s}]} I_{fs \to ap}^{(k)}\left(\mathrm{x}_{v,t}^{(k)}, \mathrm{x}_{v,r}^{(k)}, \mathrm{x}_{i,t}\right). \tag{21}$$

Similarly to (20), an average of (21) over all the possible positions of $\mathrm{x}_{v,t}^{(k)}$, $\mathrm{x}_{v,r}^{(k)}$, and $\mathrm{x}_{i,t}$ can be calculated as

$$\begin{aligned}
\bar{I}_{avg} &= \mathbb{E}\left[I_{avg}\right] \\
&= \mathbb{E}\left[\frac{1}{\mathbb{N}\left[\mathcal{S}_{5s}\right]} \sum_{k=1}^{\mathbb{N}[\mathcal{S}_{5s}]} I_{fs \to ap}^{(k)}\left(\mathrm{x}_{v,t}^{(k)}, \mathrm{x}_{v,r}^{(k)}, \mathrm{x}_{i,t}\right)\right].
\end{aligned} \tag{22}$$

C. Evaluation of Interference

Similarly to the ES-to-AP interference study, we adopt I/N as our coexistence interference metric, which is defined according to the direction of interference as

$$(\mathrm{I/N})_{ap \text{ or } ue \to fs} = \bar{I}_{aggr} / N_{th,fs} \tag{23}$$

$$(\mathrm{I/N})_{fs \to ap \text{ or } ue} = \bar{I}_{avg} / N_{th,ap \text{ or } ue} \tag{24}$$

where $N_{th,(\cdot)}$ is the thermal noise power of a receiver device according to the system type.

As mentioned in Section II, TH_{5g} of -6 and 0 dB are typically used for mobile terrestrial systems. An TH_{fs} of -10 dB was chosen for the FS as per [38].

Recall from (20) and (22) that the 5G-to-FS interference metric is aggregated whereas the FS-to-5G interference is averaged over $\mathbb{N}[\mathcal{S}_{5s}] = 57$ sectors in the 5G system. This is why 5G-to-FS interference is more significant, as observed in Figs. 10 through 13. It is shown in Figs. 10 and 11 that the 5G-to-FS interference is above the interference protection criterion of the FS, $TH_{fs} = -10$ dB of I/N, in many cases where the FS node is situated in the proximity of the 5G system. On the other hand, Figs. 12 and 13 show that the FS-to-5G interference is below the interference protection criterion of the 5G, $TH_{5g} = -6$ and 0 dB of I/N, in all cases of interest. Comparing both sets of figures, it is consistently observed that UMi yields lower interference than UMa, in both scenarios of 5G-to-FS and FS-to-5G interference. This is because UMi predicts a higher propagation loss which in turn leads to a lower interference signal power.

One interesting observation is that an *inflection point* is observed in the region of 2,000 to 4,000 m, in all of Figs. 10 through 13. To analyze this phenomenon, we consider a single AP and place it at the center of the 5G system (see Fig. 7 for

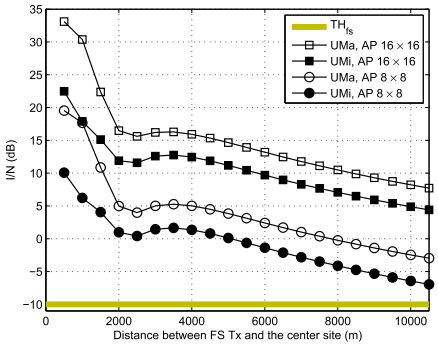

Fig. 10. Interference from 5G APs to FS.

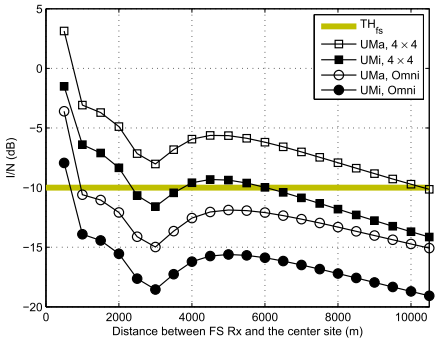

Fig. 11. Interference from 5G UEs to FS.

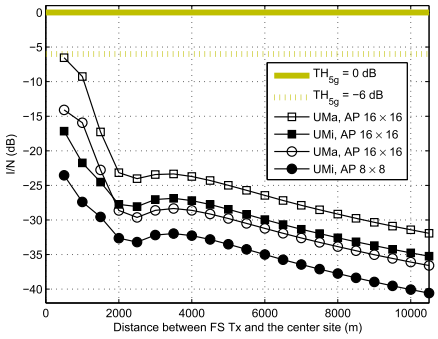

Fig. 12. Interference from FS to 5G APs.

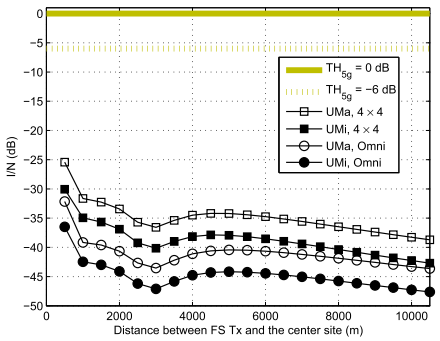

Fig. 13. Interference from FS to 5G UEs.

the layout). We found two dominant factors contributing to the AP-to-FS interference: (i) the elevation antenna gain of the FS node, $G_{fs,e}\left(\theta_{fs,off}\right)$, and (ii) the path loss from the AP to the FS as a function of distance, $PL_{5g\rightarrow fs}$. Fig. 14 shows the two factors separately, and the resulting I/N with the two factors combined. In Fig. 14a, around the region of 3,000 to 3,500 m, $G_{fs,e}\left(\theta_{fs,off}\right)$ increases by 8.35 dB while $PL_{5g\rightarrow fs}$ drops by only 2.3 dB in Fig. 14b. Therefore, in Fig. 14c, the resulting I/N increases by 5.73 dB which causes an inflection point. We note that the elevation antenna gain curve is the result of the FS antenna beam pattern model adopted by the ITU [36]. Hence, the behavior of I/N is dependent on the specific properties of the FS node antenna pattern.

IV. Mitigation of Interference From 5G Into Fixed Service

As demonstrated in Section III, in the coexistence between 5G and FS, the 5G-to-FS interference is more problematic due to aggregation of interference from multiple 5G sectors. This section proposes practical mechanisms to mitigate AP-to-FS and UE-to-FS interference. Although the proposed mechanisms refer to the system model and parameters discussed in Section III, these mechanisms can be applied to any interference scenario where a 5G system adopting high-gain steerable directional antennas coexists with a terrestrial incumbent system.

The key idea of the proposed mitigation methods is to prohibit transmissions from 5G nodes (APs or UEs) with transmit beams pointing at the victim FS receiver. In other words, the 5G transmitters are driven to point the beams away enough from the FS receiver so that they have sufficiently attenuated transmit gains toward the FS.

A. Mitigation of AP-to-FS Interference

Without loss of generality, let us consider beam restriction techniques on the azimuth plain. For an AP, $\phi_{ap,off}$ and $\phi_{ap,str}$ are recalled from Fig. 8 as an off-axis angle and a steering angle. Note that the antenna gain of an AP's beam attenuates as it: (i) points further away from the FS receiver and (ii) gets further away from the sector's physical orientation. The victim FS receiver can undergo a lower interference if the transmit beam from an AP is sufficiently attenuated based on the two factors. To measure the two types of attenuation, we define the thresholds Φ_{off} and Φ_{str} that $\phi_{ap,off}$ and $\phi_{ap,str}$ must exceed, respectively. Fig. 15 illustrates the thresholds. If a beam is with $\phi_{ap,off} \leq \Phi_{off}$, it means that the beam points closer at the FS receiver than allowed. Similarly, if $\phi_{ap,str} \leq \Phi_{str}$, the beam is attenuated less than allowed by electrical steering.

Therefore, we shut down a beam if it does not meet $\phi_{ap,off} > \Phi_{off}$ and $\phi_{ap,str} > \Phi_{str}$ at the same time, which is formulated based on (4) as

$$G_{ap}\left(\phi_{ap,off},\phi_{ap,str}\right) = \begin{cases} G_{ap}\left(\phi_{ap,off},\phi_{ap,str}\right), & \phi_{ap,off} > \Phi_{off} \\ & \text{and } \phi_{ap,str} > \Phi_{str} \\ 0, & \text{otherwise.} \end{cases} \tag{25}$$

Now, we can rewrite (16) to depict that an AP is the interfering transmitter and the FS is the victim receiver as

$$I^{(k)}_{ap\rightarrow fs} = \frac{P_{T,ap}G_{ap}\left(\phi_{ap,off},\phi_{ap,str}\right)G_{fs}\left(\phi_v,\theta_v\right)}{PL_{ap\rightarrow fs}\left(\mathrm{x}_{ap},\mathrm{x}_{fs}\right)} \tag{26}$$

where $P_{T,ap}$ denotes transmit power of an AP. Thus, an AP-to-FS interference aggregated over the $\mathbb{N}[S_{5s}] = 57$ sectors is obtained by substituting (26) into (19), which now reflects the proposed interference mitigation method.

As mentioned in Section I, this proposed method enables each AP to autonomously (without the need of an inter-system infrastructure) identify the beams that are to be avoided and perform the interference mitigation. The reason is that for the computation of Φ_{off}, the only information that an AP needs is location of the victim FS receiver. It can be learned from the license data registered to the FCC because all the FS devices in the 70 GHz band are required to register.

The proposed method is integrated into a realistic protocol that utilizes 5G interface as follows:

1) Define (a) Beam Exclusion Zone(s) at Each AP: Each AP constructs (an) exclusion zone(s), which is defined as an intersection (highlighted in light green in Fig. 15) of two fan-shaped areas that are formed by the following two inequalities: (i) $\phi_{ap,off} < \Phi_{off}$ and (ii) $\phi_{ap,str} < \Phi_{str}$.

2) Shut Down the Interfering Beams: The interfering beams are identified as the beams in the exclusion zones. Downlink pilot transmissions corresponding to these beams are also shut down (or transmitted at reduced power levels) during the 5G beam scanning intervals. This enables 5G UEs to exclude such interfering beams during their initial beam attachment or periodic beam re-selection process. A UE requesting an attachment in an exclusion zone is handed over to another sector through a re-selection process.

B. Mitigation of UE-to-FS Interference

The method of mitigating UE-to-FS interference is also a two-step process as follows:

1) Identify the Interfering UE Based on its Uplink Reference Signal: The proposed UE-to-FS interference mitigation technique is similar to the AP-to-FS interference mitigation. It aims to reduce interference caused by UEs, based on identification of the specific beams causing unacceptable interference at the FS receiver. Hence it also refers to (26), but with the parameters for the UE.

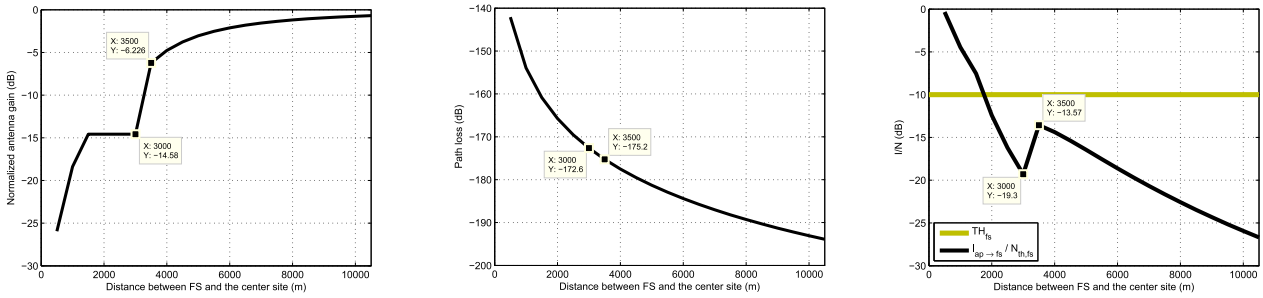

(a) $G_{fs,e}\left(\theta_{fs,off}\right)$ (b) $PL_{5g\rightarrow fs}$ (c) Resulting AP-to-FS interference

Fig. 14. Non-convexity in 5G-to-FS interference.

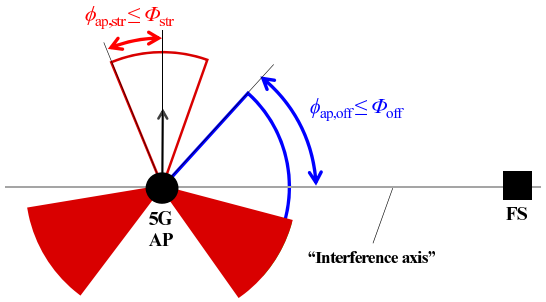

Fig. 15. Definition of exclusion zone at a 5G AP.

However, the key problem with identification of the interfering UEs is that in general only the AP is aware of which of its UEs are assigned to transmit during a certain uplink time slot. As a solution, this paper proposes a *probe-based* method where a 5G probe device is co-located with the victim FS receiver. The probe measures and reports its uplink Reference Signal Received Power (RSRP) measurements to the 5G system server. The probe device is frame-synchronized with the 5G system and may rely on the uplink 5G air-interface beam measurement procedures. Also, the antenna characteristics of the probe device should match those of the FS node (Table VI), which enables the probe to accurately track UE-generated interference as received by the FS node.

To enable interfering UE identification by the 5G system, it is proposed for the emerging 5G air interface to embed a cell-specific identification signal into the uplink Demodulation Reference Signal (DMRS). The cell-specific identification signal can take a form of a pseudo-noise (PN) sequence with a particular index of the sequence tied a particular 5G cell in which the uplink transmission was performed. Given the probe's RSRP report and the identity of the cell in which the interfering transmission has occurred, the 5G system can readily identify the interfering UE(s) by learning the particular frame and cell of the interfering transmission(s).

2) Hand Over the Interfering UEs to Another Sector: Given that the interfering UEs have been successfully detected and identified, the 5G system initiates a handover of the interfering UEs to another sector. Because of the highly directional transmit beams deployed by the 5G UEs on the uplink, simply handing over the interfering UEs will very likely change the direction of the UEs' transmit beams even if the UEs remains stationary. This change in the transmit beam direction will mitigate or even fully eliminate the interference observed at the FS node prior to the handover.

V. Evaluation of the Proposed Interference Mitigation Technique

We evaluate performance of the interference mitigation methods that are discussed in Section IV. The settings and parameters for the evaluation refer to Table VI of Section IV.

A. Evaluation Method

We assess the proposed interference mitigation techniques in the following two aspects: (i) 5G-to-FS interference and (ii) impact on performance of the 5G system itself. Firstly, the improvement in the 5G-to-FS interference is calculated based on (23). Secondly, the application of the proposed AP and UE interference mitigation methods will invariably lead to performance degradation of the 5G system, since the AP interference mitigation technique restricts the selection of beams available for UE attachment on the downlink and forces handover to a possibly suboptimum attachment point for the UE interference mitigation on the uplink. We characterize this performance degradation by computing downlink SINR and uplink SNR before and after applying the downlink and uplink interference mitigation techniques.

For the downlink, a signal-to-interference-plus-noise ratio (SINR) that is measured at a UE in the jth sector, $\mathcal{R}_j^2$, is calculated as

$$\text{SINR} = \frac{P_{R,ue}^{(j)} G_{ue} G_{ap}}{N_{th,ue} + \sum_{k \in \mathbb{N}[\mathcal{S}_{5s}], k \neq j} P_{R,ue}^{(k)}}. \tag{27}$$

where $P_{R,ue}^{(j)}$ denotes the signal power that the UE receives from the jth sector's antenna. Note that this SINR does not include the interference from the FS; referring to Fig. 12, the FS-to-AP interference is insignificant compared to the noise level observed at the UEs.

For the uplink, a signal-to-noise ratio (SNR) at an AP is obtained as

$$\text{SNR} = \frac{P_{R,ap}^{(j)} G_{ap} G_{ue}}{N_{th,ap}}. \tag{28}$$

where $P_{R,ap}^{(j)}$ denotes a signal power received at the jth sector. Similarly, the FS-to-UE interference is excluded since it has

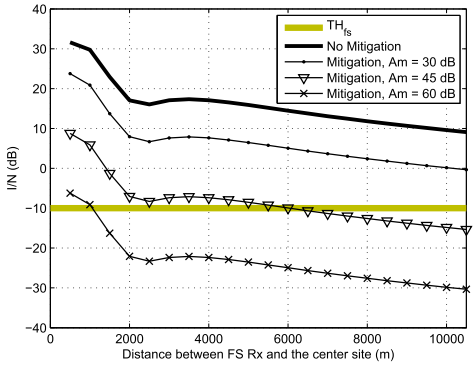

Fig. 16. Mitigation of AP-to-FS interference.

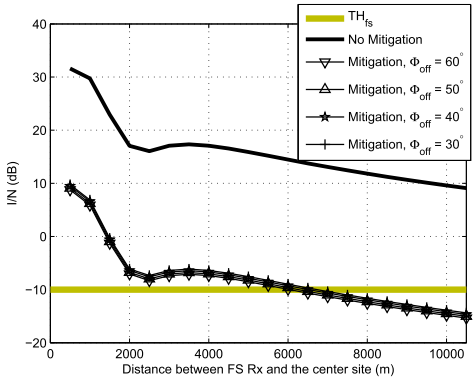

Fig. 17. Reduction of Φ_{off} ($\Phi_{str} = 60°$, $A_m = 45$ dB).

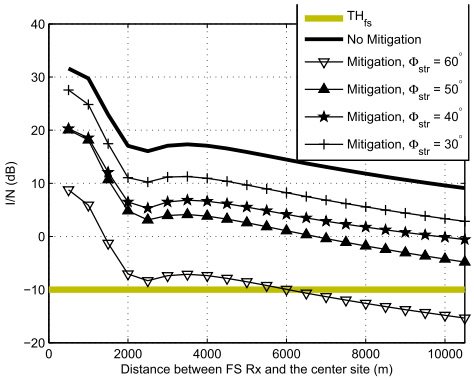

Fig. 18. Reduction of Φ_{str} ($\Phi_{off} = 60°$, $A_m = 45$ dB).

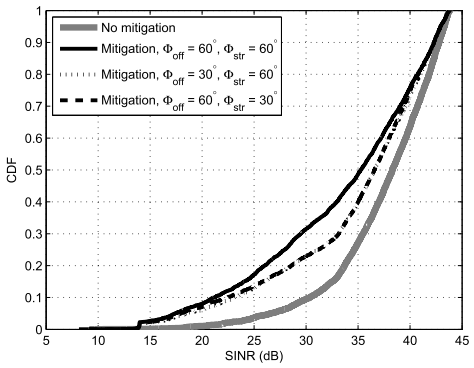

Fig. 19. Impact of Φ_{off} and Φ_{str} on the 5G downlink SINR.

little impact on the SNR as observed from Fig. 13. As a further simplification, we note that the uplink performance is noise-limited due to lower UE transmit powers and also exclude inter-cell interference from calculation of the uplink SNR.

B. AP-to-FS Interference Mitigation

Fig. 16 shows the impact of the proposed interference mitigation technique on the AP-to-FS interference. Note that the decrease in AP-to-FS interference follows the corresponding increase in sector antenna's front-to-back ratio, A_m; this is especially pronounced in the region of AP-to-FS distance of 2,000 m or more. That is, a 15 dB increase in A_m roughly results in a 15 dB decrease in I/N. This effect demonstrates that the dominant interfering beams in the sectors that are pointed directly at the FS node have been suppressed and the interference is now largely dependent on the power received from the sectors that are pointed away from the FS node.

As the performance of the 5G system can be adversely affected by the size of a beam exclusion zone, here we explore the sensitivity of the resulting I/N at the FS node to the size of the exclusion zone at an AP. Reduction of exclusion zone can be achieved by reduction of either Φ_{off} or Φ_{str}, defined above in Fig. 15. Impacts of reduction of the two thresholds are shown in Figs. 17 and 18. Reducing the exclusion zone according to Φ_{off} does not result in a significant increase in AP-to-FS interference, as shown in Fig. 17. On the other hand, Fig. 18 shows that reduction of exclusion zone according to Φ_{str} significantly increases AP-to-FS interference.

The reason for this behavior is explained in Fig. 20. Each subfigure shows a cumulative snapshot of 10 drops with 10 UEs dropped per sector. For consistency with the topology shown in Fig. 15, the victim FS node is fixed at $(x, y) = (500, 0)$ which is on the right side of the cell; thus the interference axis is defined as a horizontal line passing through the AP at $(0, 0)$ in each subfigure. The red dots represent the UEs in the exclusion zone, while the blue ones indicate those outside of the zone where downlink transmissions are allowed. Let us begin with the case of $\Phi_{off} = 60°, \Phi_{str} = 60°$ that is given in Fig. 20a. The cases where the thresholds Φ_{off} and Φ_{str} are reduced are presented in Figs. 20b and 20c, respectively. In Fig.20b, reduction of Φ_{off} opens up a beam transmission area that is further away from the interference axis, which does not translate into increased interference at the FS node. On the other hand, in Figs. 20c, reduction of ϕ_{str} opens up an area with interfering beam transmissions that is closer to the interference axis, resulting in significant interference increase at the FS node.

We further note that reducing either of the two thresholds results in a similar level of improvement in SINR for the 5G downlink which is given in (27). Fig. 19 displays a CDF of the downlink SINRs with no interference mitigation and three different Φ_{off} and Φ_{str} settings. The figure shows that reduction of either Φ_{off} or Φ_{str} improves the SINRs since both of these thresholds about equally reduce the beam exclusion zone at each AP. This is also evident in Figs. 20b and 20c, where the sizes of the exclusion zones (areas with red dots) are roughly equal after reduction. As a consequence, it is much more efficient to adjust Φ_{off} for controlling the size of

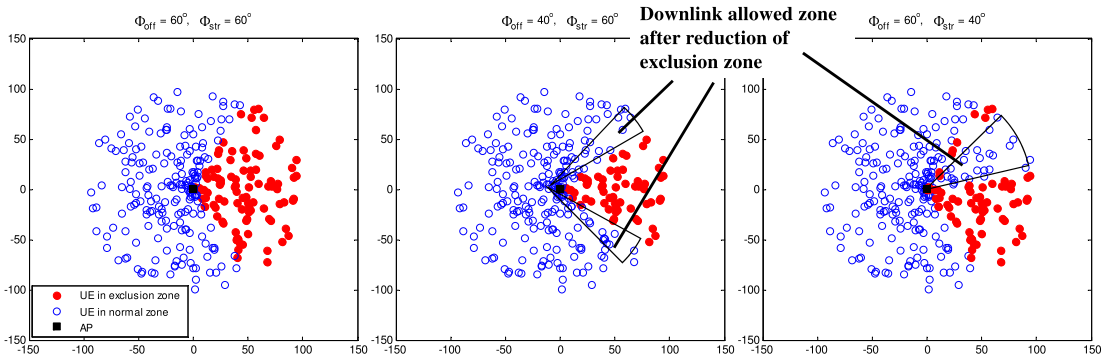

(a) $\Phi_{off} = 60°, \Phi_{str} = 60°$ (b) $\Phi_{off} = 40°, \Phi_{str} = 60°$ (c) $\Phi_{off} = 60°, \Phi_{str} = 40°$

Fig. 20. Example of reduction of the thresholds, Φ_{off} and Φ_{str}.

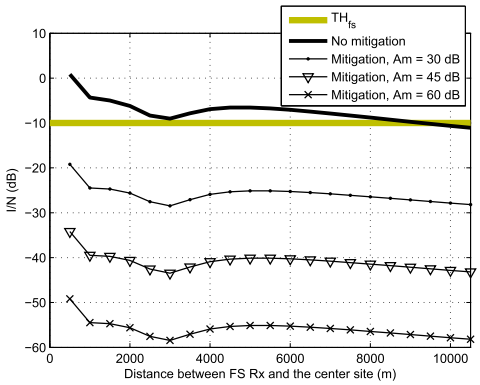

Fig. 21. Mitigation of UE-to-FS interference.

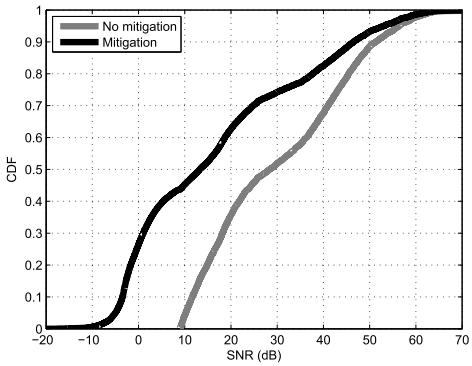

Fig. 22. Impact of UE-to-FS interference mitigation on the 5G uplink SNR.

the exclusion zone, while keeping Φ_{str} fixed, since adjusting Φ_{off} yields a similar level of downlink SINR improvement but without increasing the AP-to-FS interference.

C. UE-to-FS Interference Mitigation

Fig. 21 evaluates the UE-to-FS interference with application of the proposed mitigation technique. Similar to the trend observed in Fig. 16, the change in residual interference level observed at the FS node roughly follows the change in the UEs' antenna front-to-back ratio, A_m. We again conclude that the proposed mitigation technique on the UE side is effective in suppression of the beams pointed directly at the FS node, as it is observed that the residual interference becomes a function of the energy received from the back side of a UE's antenna.

Fig. 22 presents the impact of the UE-to-FS interference mitigation technique on the uplink 5G system performance. Maximum degradation observed with this mitigation technique is approximately 15 dB, which is due to forcing the interfering UEs to re-attach to a sector that provides a sub-optimum uplink signal strength.

D. Discussion on Performance of 5G

In general, 5G systems will be expected to provide a high degree of coverage and reliability even in the most severe propagation environments. In [20], typical values of SINR for uplink and downlink at mmW frequencies are displayed. According to the results in [20], SINRs as low as -10 dB could be observed at these frequencies in challenging propagation conditions, and 5G systems are expected to remain fully operational even in these very low SINR conditions.

From Figs. 19 and 22, one can see that the "worst-case" downlink SINR and uplink SNR of a 5G system adopting the proposed interference mitigation techniques are also in the range of -10 dB. Thus, we conclude that despite some degradation in both downlink and uplink due to incumbent interference mitigation, the performance of a 5G system will remain acceptable.

VI. Conclusion

This paper performed a detailed analysis of coexistence scenarios for 5G in mmW bands, namely co-channel coexistence of 5G with FSS uplink at 28 GHz and with FS WB at 70 GHz. The first part of our 28 GHz study discussed the AP-to-SS and UE-to-SS interference. We showed that 5G can satisfy interference protection criteria of the FSS while allowing simultaneous transmissions from at least several thousands of sectors and tens of thousands of UEs under various LoS and NLoS channel conditions and with various sets of parameters for the FSS. In the analysis of ES-to-AP interference, we characterized the separation distances in order to guarantee that higher than 95% of uplink transmissions in the nearest cell are protected. The required separation

distances are not overly restrictive for deployment of 5G systems, and our results further validate that the 28 GHz band is viable for future 5G system deployments. In the 70 GHz study, we demonstrated that the 5G-to-FS interference is more significant than the FS-to-5G interference, due to aggregation of interference among all of the sectors. Motivated by this observation, we proposed the mechanisms that mitigate the interference from APs and UEs into the FS system. Our results showed that the proposed techniques can effectively suppress the interference at the FS receiver while maintaining operable performance of 5G.

REFERENCES

[1] Z. Pi and F. Khan, "An introduction to millimeter-wave mobile broadband systems," *IEEE Commun. Mag.*, vol. 49, no. 6, pp. 101–107, Jun. 2011.

[2] C. T. Neil, M. Shafi, P. J. Smith, and P. A. Dmochowski, "On the impact of antenna topologies for massive MIMO systems," in *Proc. IEEE ICC*, Jun. 2015, pp. 2030–2035.

[3] C. T. Neil, M. Shafi, P. J. Smith, and P. A. Dmochowski, "Deployment issues for massive MIMO systems," in *Proc. IEEE ICC*, Jun. 2015, pp. 1298–1303.

[4] *Report and Order and Second Further Notice of Proposed Rulemaking, in the Matter of Amendment of the Commission's Rules With Regard to Commercial Operations in the 3550–3650 MHz Band*, document GN Docket 12-354, FCC, Washington, DC, USA, Apr. 2015.

[5] *Report and Order and Second Further Notice of Proposed Rulemaking, Use of Spectrum Bands Above 24 GHz for Mobile Radio Services*, document GN Docket 14–177, FCC, Washington, DC, USA, Jul. 2016.

[6] *Resolution COM6/20: Studies on Frequencyrelated Matters for International Mobile Telecommunications Identification Including Possible Additional Allocations to the Mobile Services on a Primary Basis in Portion(s) of the Frequency Range Between 24.25 and 86 GHz for the Future Development of International Mobile Telecommunications for 2020 and Beyond*, World Radiocommunication Conference (WRC15), Geneva, Switzerland, 2015.

[7] A. Khawar, A. Abdelhadi, and T. C. Clancy, "A mathematical analysis of cellular interference on the performance of S-band military radar systems," in *Proc. Wireless Telecommun. Symp. (WTS)*, Apr. 2014, pp. 1–8.

[8] Y. Noam and A. J. Goldsmith, "Blind null-space learning for MIMO underlay cognitive radio with primary user interference adaptation," *IEEE Trans. Wireless Commun.*, vol. 12, no. 4, pp. 1722–1734, Apr. 2013.

[9] K. W. Sung, M. Tercero, and J. Zander, "Aggregate interference in secondary access with interference protection," *IEEE Commun. Lett.*, vol. 15, no. 6, pp. 629–631, Jun. 2011.

[10] P. A. Dmochowski, P. J. Smith, M. Shafi, J. G. Andrews, and R. Mehta, "Interference models for heterogenous sources," in *Proc. IEEE ICC*, Jun. 2012, pp. 4049–4054.

[11] M. Ghorbanzadeh, E. Visotsky, P. Moorut, W. Yang, and C. Clancy, "Radar inband and out-of-band interference into LTE macro and small cell uplinks in the 3.5 GHz band," in *Proc. IEEE WCNC*, Mar. 2015, pp. 1829–1834.

[12] J. H. Reed *et al.*, "On the co-existence of TD-LTE and radar over 3.5 GHz band: An experimental study," *IEEE Wireless Commun. Lett.*, vol. 5, no. 4, pp. 368–371, Aug. 2016.

[13] M. Tercero, K. W. Sung, and J. Zander, "Impact of aggregate interference on meteorological radar from secondary users," in *Proc. IEEE WCNC*, Mar. 2011, pp. 2167–2172.

[14] F. Hessar and S. Roy, "Spectrum sharing between a surveillance radar and secondary Wi-Fi networks," *IEEE Trans. Aerosp. Electron. Syst.*, vol. 52, no. 3, pp. 1434–1448, Jun. 2016.

[15] E. Obregon, K. W. Sung, and J. Zander, "On the sharing opportunities for ultra-dense networks in the radar bands," in *Proc. IEEE DYSPAN*, Apr. 2014, pp. 215–223.

[16] E. Obregon, K. W. Sung, and J. Zander, "Exploiting temporal secondary access opportunities in radar spectrum," *Wireless Pers. Commun.*, vol. 72, no. 3, pp. 1663–1674, Mar. 2013.

[17] S. Kim, J. Choi, and C. Dietrich, "PSUN: An OFDM-pulsed radar coexistence technique with application to 3.5 GHz LTE," *Hindawi Mobile Inf. Syst.*, vol. 2016, 2016, Art. no. 7480460.

[18] S.-S. Raymond, A. Abubakari, and H.-S. Jo, "Coexistence of power-controlled cellular networks with rotating radar," *IEEE J. Sel. Areas Commun.*, vol. 34., no. 10, pp. 2605–2616, Oct. 2016.

[19] A. Lackpour, M. Luddy, and J. Winters, "Overview of interference mitigation techniques between WiMAX networks and ground based radar," in *Proc. IEEE WOCC*, Apr. 2011, pp. 1–5.

[20] M. Akdeniz *et al.*, "Millimeter wave channel modeling and cellular capacity evaluation," *IEEE J. Sel. Areas Commun.*, vol. 32, no. 6, pp. 1164–1179, Jun. 2014.

[21] F. Guidolin and M. Nekovee, "Investigating spectrum sharing between 5G millimeter wave networks and fixed satellite systems," in *Proc. IEEE Globecom*, Dec. 2015, pp. 1–7.

[22] G. R. MacCartney, Jr., and T. S. Rappaport, "73 GHz millimeter wave propagation measurements for outdoor urban mobile and backhaul communications in New York City," in *Proc. IEEE ICC*, Jun. 2014, pp. 4862–4867.

[23] O. Holland and M. Dohler, "Geolocation-based architecture for heterogeneous spectrum usage in 5G," in *Proc. IEEE Globecom*, Dec. 2015, pp. 1–6.

[24] D. A. Wassie, G. Berardinelli, F. M. L. Tavares, T. B. Sorensen, and P. Mogensen, "Experimental verification of interference mitigation techniques for 5G small cells," in *Proc. IEEE VTC Spring*, May 2015, pp. 1–5.

[25] T. K. Vu, M. Bennis, S. Samarakoon, M. Debbah, and M. Latva-Aho, "Joint in-band backhauling and interference mitigation in 5G heterogeneous networks," in *Proc. IEEE Eur. Wireless*, May 2016, pp. 1–6.

[26] G. Li, T. Irnich, and C. Shi, "Coordination context-based spectrum sharing for 5G millimeter-wave networks," in *Proc. IEEE CROWNCOM*, Jun. 2014, pp. 32–38.

[27] D. Stoyan *et al.*, *Stochastic Geometry and its Applications*, vol. 2. Chichester, U.K.: Wiley, 1995.

[28] *International Telecommunications Union*, document ITU-R P.525, Dec. 2016.

[29] Verizon, AT&T, Nokia, Ericsson, Samsung, and T-Mobile, "Letter to Federal Communications Commission on GN Docket No. 14-177 and IB Docket No. 15-256," Tech. Rep., May 2016.

[30] H. Anderson, *Fixed Broadband Wireless System Design*. Hoboken, NJ, USA: Wiley, 2003.

[31] *International Telecommunications Union*, document ITU-R S.1432, Apr. 2016.

[32] *International Telecommunications Union*, document ITU-R M.2030, 2003.

[33] [Online]. Available: http://www.vcomm-eng.com/wp-content/uploads/2014/01/12-35704-18-2013Verizon7022285928.pdf

[34] *Antenna Performance Standards*, document 47 CFR 25.209, FCC, Washington, DC, USA, 2010. [Online]. Available: https://www.gpo.gov/fdsys/granule/CFR-2010-title47-vol2/CFR-2010-title47-vol2-sec25-209

[35] *Channel Model for Frequency Spectrum Above 6 GHz (Release 14)*, document TR 38.900, v1.0.0, 3GPP, Jun. 2016.

[36] *International Telecommunications Union*, document ITU-R F.699-7, Dec. 2010.

[37] *Further Advancements for E-UTRA Physical Layer Aspects*, document TR 36.814 (Release 9), 3GPP, Sophia-Antipolis, France, 2010.

[38] *International Telecommunications Union*, document ITU-R F.758-6, Sep. 2015.

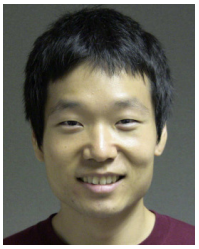

Seungmo Kim received the B.S. and M.S. degrees in electrical communications engineering from the Korea Advanced Institute of Science and Technology, Daejeon, South Korea, in 2006 and 2008, respectively. He is currently pursuing the Ph.D. degree with the Bradley Department of Electrical and Computer Engineering, Virginia Polytechnic Institute and State University, Blacksburg, VA, USA. His current research interests include the coexistence of heterogeneous wireless systems and efficient communications protocols for Internet of Things applications. He was a recipient of the Best Paper Award at the IEEE WCNC 2016 International Workshop on Smart Spectrum.

Eugene Visotsky (M'12) received the B.S., M.S., and Ph.D. degrees from the University of Illinois at Urbana–Champaign, in 1996, 1998, and 2000, respectively, all in electrical engineering. In 2000, he joined the Communication Systems Research Laboratory, Motorola Labs, Schaumburg, IL, USA. Since 2011, he has been with Nokia Bell Labs, where is involved in advanced signal processing techniques for spread spectrum communication systems, link adaptation, multicarrier modulation techniques, and multihop protocols applied in cellular systems. He has authored or co-authored a number of issued and pending U.S. patents. His current research interests include advanced inter-cell interference coordination, cooperative transmission algorithms, 3D MIMO techniques, and 5G coexistence issues.

Prakash Moorut received the M.S.E.E. degree from École Supérieure d'Electricité, Paris, France. He is currently the North America Spectrum Lead with Nokia Bell Labs, where he is involved in regulators, operators, and industry members to open more useable commercial spectrum in North America. Prior joining Nokia Bell Labs, he was with Motorola, where he created and led a Customer Facing Spectrum Engineering Group, in USA, France, and China. He has over 19 years of experience in Europe and USA on numerous wireless communications system, including GSM, CDMA, UMTS, TETRA/Public Safety, WiMAX, LTE, LTE-Advanced, and is currently enabling Small Cells, 5G technologies, and Spectrum Sharing. He also has extensive experience in spectrum regulation and strategy, standardization, spectrum coexistence analysis/simulations and developing efficient spectrum usage solutions for products and operators worldwide. He has earned industry recognition and is regularly invited to speak at various FCC workshops and other venues about spectrum management. He holds several publications and patents related to spectrum usage.

Kamil Bechta received the M.Sc. degree in electronics engineering from the Military University of Technology, Warsaw, Poland, in 2010. He was a Research Assistant with the Military University of Technology and in 2011 he joined Nokia Siemens Networks as a 3GPP RAN4 Standardization Specialist, where he was involved in the RF and RRM requirements of HSPA and LTE. Since 2015, he has been a 5G Senior Radio Research Engineer with Nokia Bell Labs, he has been leading the team and responsible for spectrum and co-existence studies for 5G. Since 2017, he has been a Senior System Engineer, where he was involved in the development of advanced baseband platforms in Nokia.

Amitava Ghosh (F'15) received the Ph.D. degree in electrical engineering from Southern Methodist University, Dallas, TX, USA. He joined Motorola, in 1990, after his Ph.D. Since joining Motorola, he was involved in multiple wireless technologies from IS-95, cdma-2000, 1xEV-DV/1XTREME, 1xEV-DO, UMTS, HSPA, 802.16e/WiMAX, and 3GPP LTE. He is currently a Nokia Fellow and the Head of Small Cell Research with the Nokia Bell Labs. He is currently involved in 3GPP LTE-Advanced and 5G technologies. He has co-authored a book *Essentials of LTE and LTE-A*. He holds 60 issued patents, has written multiple book chapters, and has authored numerous external and internal technical papers. His research interests are in the area of digital communications, signal processing, and wireless communications. He was a recipient of the 2016 IEEE Stephen O. Rice Prize.

Carl Dietrich (SM'13) received the B.S. degree in electrical engineering from Texas A&M University, College Station, TX, USA, and the Ph.D. and M.S. degrees from the Bradley Department of Electrical and Computer Engineering, Virginia Polytechnic Institute and State University, Blacksburg, VA, USA. He is also a Licensed Professional Engineer in Virginia. His current research interests include spectrum sharing, cognitive radio, software defined radio, multi-antenna systems, and radio wave propagation. He has chaired the Wireless Innovation Forums Educational Special Interest Group, and is a member of the IEEE Eta Kappa Nu and ASEE.